Measurement of absolute differential excitation cross sections of molecular oxygen by electron impact: Decomposition of the Herzberg pseudocontinuum

Tong W. Shyn and Christopher J. Sweeney*
Space Physics Research Laboratory, University of Michigan, Ann Arbor, Michigan 48109-2143
(Received 24 January 2000; published 19 July 2000)

Using a crossed-beam method, we have measured electron energy-loss spectra for excitation of the Herzberg pseudocontinuum of molecular oxygen. The scattering angle and electron-impact energy ranges covered were from 12° to 156° and from 10 to 30 eV, respectively. We decomposed the spectra into contributions from three superposed Gaussian line shapes by means of computerized least-squares analysis. The three line shapes were identified as representing excitation of the $A\,^3\Sigma_u^+$, $A'\,^3\Delta_u$, and $c\,^1\Sigma_u^-$ states. Absolute differential and integrated cross sections for all three states' excitations were obtained, along with linear electronic potential-energy curves for the Franck-Condon region.

PACS number(s): 34.80.Gs

I. INTRODUCTION

On account of its abundance in the Earth's atmosphere and its importance in a variety of biological, chemical, and physical processes, one would expect substantial research to have been done on the oxygen molecule. This is generally true for optical measurements and theoretical calculations [1,2], but relatively little research has been done on the low-energy electron-impact excitation of O_2. As shown in the reviews by Trajmar, Register, and Chutjian [3], by Trajmar and Cartwright [4], by Itikawa *et al.* [5], and by Zecca, Karwasz, and Brusa [6], the data here can been characterized as fragmentary at best. Assignment of the observed transitions is incomplete and there are gaps in the impact energy and angular ranges for the measured cross sections. This is particularly true for the Herzberg pseudocontinuum, which is composed of the $A\,^3\Sigma_u^+$, $A'\,^3\Delta_u$, and $c\,^1\Sigma_u^-$ states, and lies between about 4 and 7 eV excitation energy [7–9].

Konishi *et al.* made integral-excitation cross-section measurements for the pseudocontinuum [10]. Differential-excitation cross-section measurements of the pseudocontinuum were later done by Wakiya [11,12]. He used an energy resolution of about 200 meV and an angular range of 5°–130° to obtain cross sections summed over all three states in the pseudocontinuum region. Based on the trends in angle and impact energy exhibited by his results, he posited the $c\,^1\Sigma_u^-$ state to be the dominant one excited by electron impact below about 100 eV incident energy, in agreement with the previous assignment of Trajmar, Williams, and Kuppermann [13]. Teillet-Billy, Malegat, and Gauyacq studied the electron-impact excitation of the pseudocontinuum both experimentally and theoretically, and concerned themselves with the role of the $O_2^-(^2\Pi_g)$ resonance in the excitation process [14]. They treated only the scattering angle of 90°, and used the impact energy range from 10 to 20 eV. Unfortunately, none of these researchers tried to decompose their spectra into contributions from the underlying states. Such a decomposition would be interesting from the point of view of pure physics and chemistry because the excitations here are all forbidden, and electron impact is well known for its ability to excite forbidden transitions. It would also be useful in atmospheric science, as the $c\,^1\Sigma_u^-$ state has been postulated to be important in the series of reactions leading to the red atomic oxygen emissions observed in the Earth's atmosphere [15–19].

In this article, we present the results of decomposition of low-energy electron-impact spectra of the pseudocontinuum. A total of more than 650 energy-loss spectra were measured, covering the scattering angle and impact energy ranges of 12°–156° and 10–30 eV, respectively. The data was analyzed by means of a computerized least-squares technique. This analysis yielded absolute differential-excitation cross sections for each state, along with an approximation for each state's potential-energy curve in the Franck-Condon region. Absolute integrated cross sections were obtained from the differential ones. Our results are compared with those of others.

II. EXPERIMENT

The apparatus and procedures used for our measurements of the pseudocontinuum region were essentially the same as

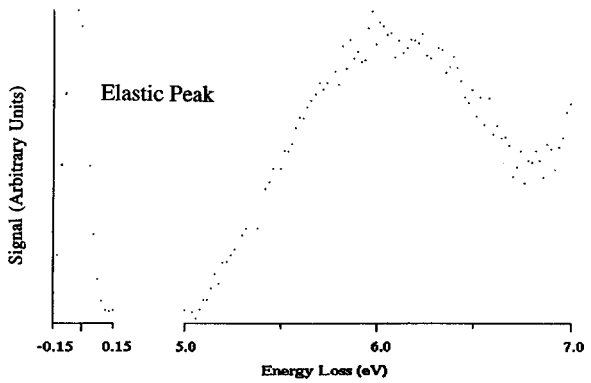

FIG. 1. A typical electron energy-loss spectrum for excitation of the pseudocontinuum by electron impact. The scattering angle was 72°, while the impact energy was 10 eV. Note the contribution on the right-hand side from the Schumann-Runge continuum.

*Also at the Department of Physics, University of Michigan, Ann Arbor, MI 48109-1120.

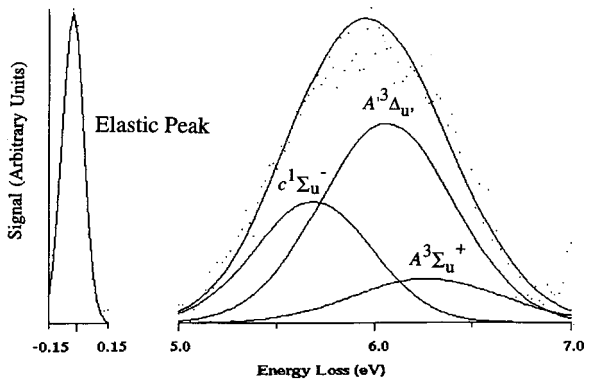

FIG. 2. The same electron energy-loss spectrum as in Fig. 1, but with the low-energy tail of the Schumann-Runge continuum removed. Fits to each state's excitation are shown. The unlabeled curve is the sum of their excitations.

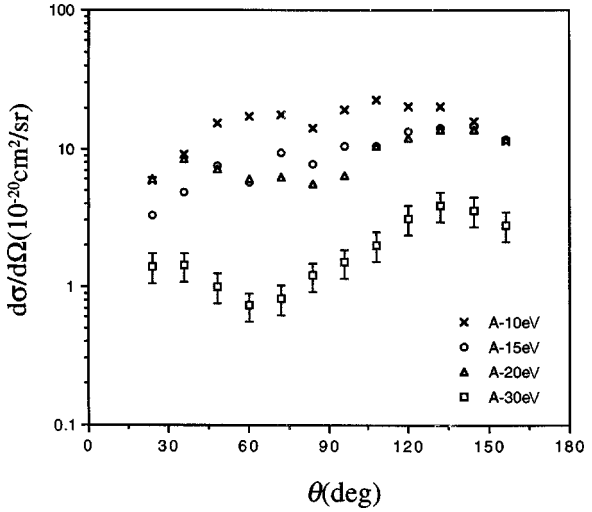

FIG. 3. Absolute differential cross sections for excitation of the $A\,^3\Sigma_u^+$ state of molecular oxygen by electron impact.

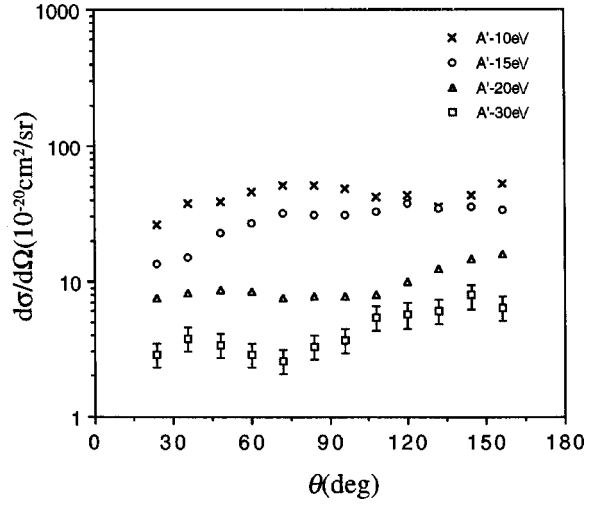

FIG. 4. Absolute differential cross sections for excitation of the $A'\,^3\Delta_u^-$ state of molecular oxygen by electron impact.

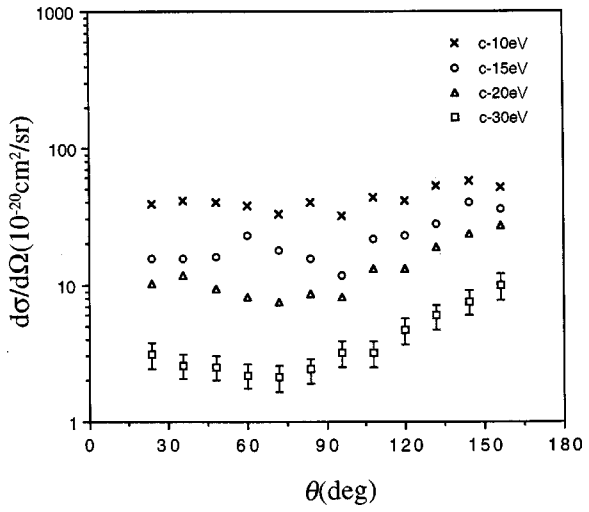

FIG. 5. Absolute differential cross sections for excitation of the $c\,^1\Sigma_u^-$ state of molecular oxygen by electron impact.

those utilized for our previous electron $-O_2$ scattering experiments [20–25], and are given detailed accounts elsewhere in the physics literature [26–28]. We thus provide only a terse account of them here. Comprising our apparatus are three principal subsystems: a neutral-molecular-oxygen-beam source, a monoenergetic electron-beam source, and a scattered-electron detector. All three subsystems are housed in a high-vacuum enclosure that is divided into differentially pumped upper and lower chambers. Three orthogonal sets of Helmholtz coils surround the vacuum enclosure to reduce stray magnetic fields—including the Earth's—to less than 20 mG in all directions in the interaction region. The energy scale of our measuring apparatus was calibrated via the 19.35-eV resonance of helium.

The neutral-molecular-oxygen-beam source resides in the upper chamber. Research grade O_2 is piped into this chamber from a commercial storage cylinder. The piping terminates at

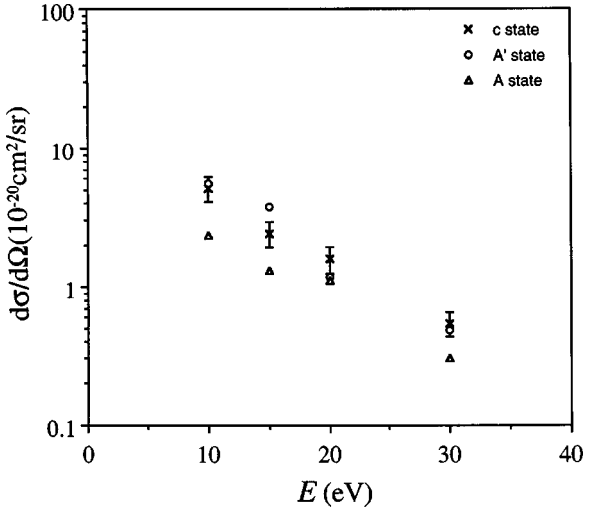

FIG. 6. Absolute integrated cross sections for excitation of the $A\,^3\Sigma_u^+$, $A'\,^3\Delta_u$, and $c\,^1\Sigma_u^-$ states of molecular oxygen by electron impact.

TABLE I. Uncertainty percentages in our measurements.

State	$c\,^1\Sigma_u^-$	$A'\,^3\Delta_u$	$A\,^3\Sigma_u^+$
Source of uncertainty			
Raw data (statistics)	5	5	7
Line shape	10	10	15
Detector efficiency	10	10	10
Elastic cross sections	14	14	14
Total	21	21	24

a capillary array positioned at the interface between the two chambers. A vertically collimated molecular beam is thus provided in the lower chamber, where the electron-molecule collisions occur.

The electron-beam source is mounted on a turntable in the lower chamber, and can be rotated from $-90°$ to $+160°$ in a continuous fashion. Comprising the beam source are an electron gun with a thoriated-iridium filament, a 127° cylindrical energy selector, two electron lens systems, and two beam deflectors. Currents in excess of 10^{-8} A are produced by this subsystem, while the angular divergence of the electron beam is approximately $\pm 3°$.

Also residing in the lower chamber is our scattered-electron detector. The detector is made of a 127° cylindrical and a hemispherical energy analyzer in series, two electron lens systems, and a Channeltron electron multiplier. This arrangement provides a signal-to-noise ratio more than 100 times better than the single-analyzer system we have employed in the past.

We know from our previous experiments that the line shape that characterizes our overall machine response (i.e., the energy profile of the electron beam convolved with the detector's response function) is well represented as Gaussian in energy, and for the present set of measurements, was fixed at about 90 meV full width at half maximum (FWHM). Note that such an energy resolution allows us to resolve vibrational and nonoverlapping electronic excitations, but not rotational excitations.

During actual measurements, the impact energy and scattering angle were fixed, while a dedicated microcomputer swept the energy-acceptance window of the detector over the region of interest and also accumulated the data. The system's electronics are stable to within a few meV per day to accommodate the often long data collection times required.

TABLE II. Mean excitation energies V_0 and slopes g for the states comprising the pseudocontinuum, along with the results of Klotz and Peyerimhoff.

State	V_0 (present result)	V_0 (Klotz and Peyerimhoff)	γ (present result)	γ (Klotz and Peyerimhoff)
$A\,^3\Sigma_u^+$	6.27	6.28	−10.14	−15
$A'\,^3\Delta_u$	6.06	6.12	−9.06	−15
$c\,^1\Sigma_u^-$	5.72	5.75	−7.94	−15

We repeated our measurement process over the prescribed impact energy and angular ranges. The results are electron energy-loss spectra like the one shown in Fig. 1.

III. DATA ANALYSIS

Our data-analysis technique was based on the original molecular line shape arguments of Franck [29] and Condon [30,31] for the vertical excitation of repulsive states. They showed that if the transition moment μ were constant with respect to the internuclear separation r, then the repulsive-excitation line shape's form is obtained from changing variables from r in the internuclear probability density to excitation energy E. The relationship between these two variables is given by the form of the internuclear potential-energy curve for the involved excited state. In position space, the internuclear ground-state probability density is to very good approximation a Gaussian—with a FWHM of quite nearly 0.086 Å for O_2. To good approximation, the involved repulsive-state potential-energy curves are linear in the Franck-Condon region for O and their transition moments vary by only a few percent [32–35]. The excitation line shapes are therefore well approximated by Gaussians, with mean energies V_0 giving the value of their potential-energy curves at ground-state internuclear equilibrium separation. The ratios γ of their FWHM's to the ground-state internuclear density's give the slopes of these curves.

The analysis of our pseudocontinuum data thus consists of fitting three Gaussians to each energy-loss spectrum, since there are three superposed states involved. To do this, we chose model spectra of the form

$$s(\rho,S_0,\theta,E_i,E_l)=\rho S_0 G(\theta)\epsilon(E_i-E_l)\times\sum_{j=1}^{N} F_j(E_i-E_l)I_j(\theta,E_i)+B(E_i-E_l), \quad (1)$$

TABLE III. Absolute cross sections for the excitation of the $A\,^3\Sigma_u^+$ state of molecular oxygen by electron impact. Units for the differential cross sections are $10^{-20}\,\mathrm{cm}^2/\mathrm{sr}$, while those for the integrated cross sections are $10^{-18}\,\mathrm{cm}^2$. Parentheses enclose extrapolated values.

E (eV) \ θ (deg)	12	24	36	48	60	72	84	96	108	120	132	144	156	168	σ
10	(4.5)	6.0	9.2	15.7	17.6	17.9	19.3	14.2	22.8	20.6	20.8	16.0	11.4	(8.0)	2.34
15	(2.5)	3.3	4.8	6.2	5.7	9.4	7.9	10.7	10.7	13.7	14.3	14.7	11.7	(10)	1.31
20	(4.0)	6.0	8.5	7.2	6.0	6.2	5.7	6.3	10.7	12.0	14.1	13.8	12.0	(10)	1.11
30	(1.2)	1.4	1.4	1.0	0.7	0.8	1.2	1.5	2.0	3.1	3.9	3.6	2.8	(2.0)	0.25

TABLE IV. Absolute cross sections for the excitation of the $A'\,^3\Delta_u$ state of molecular oxygen by electron impact. Units for the differential cross sections are $10^{-20}\,\mathrm{cm}^2/\mathrm{sr}$, while those for the integrated cross sections are $10^{-18}\,\mathrm{cm}^2$. Parentheses enclose extrapolated values.

E (eV) \ θ (deg)	12	24	36	48	60	72	84	96	108	120	132	144	156	168	σ
10	(20)	26.2	38.2	38.8	45.5	50.8	51.7	48.9	42.7	44.1	35.6	43.9	52.8	(55)	5.55
15	(11)	13.6	15.3	22.7	26.9	32.5	30.8	31.3	33.4	37.7	35.1	35.7	34.3	(33)	3.75
20	(6.5)	7.6	8.3	8.8	8.4	7.6	7.8	7.8	8.0	10.0	12.4	14.9	16.0	(17)	1.19
30	(3.5)	2.9	3.8	3.4	2.9	2.6	3.3	3.7	5.5	5.7	6.1	7.9	6.5	(7.5)	0.56

where s is the scattered-electron signal, ρ the molecular-beam density, and S_0 the incident electron current. $G(\theta)$ is a factor describing the scattering geometry, E_i the impact energy, and E_l the electron energy loss. For the $N=3$ states the F_j's are the Gaussians, and have fixed values of one at their maxima. Differences in excitation intensity among the states are accounted for in the values of the $I_j s$. B is a term representing the background, and included contributions from the nearby strong excitation of the Schumann-Runge continuum [25]. Before any fitting was done, our measured spectra were corrected for the effects of nonconstant detection efficiency ϵ with respect to energy. We note that the magnitudes of the cross sections for the individual states' excitations are strongly dependent on the least-squares data reduction and background removal technique, as the excitations are not resolvable in the spectra.

The fitting was performed numerically by the traditional least-squares minimization approach, and the algorithm we employed for this purpose was the method of simulated annealing implemented through the use of downhill simplexes. The FORTRAN90 program we used for this purpose was based heavily on the original source code of Press and Teukolsky [36]. We chose the simulated-annealing algorithm because, though it is generally less efficient than the traditional steepest-descents approaches, it has the advantage over these that it does not get ''stuck'' in local minima in parameter space, and therefore can locate the true global minimum among the many local minima often present [37].

The fitting is complicated a little by the fact that the measured-excitation spectra are broadened from the natural-excitation spectra by the machine response of our system. Since this machine response is Gaussian, we can analytically perform the convolution integral of it with the natural Gaussian line shape to obtained measured-excitation line shapes also Gaussian in form [38]. With $\Delta_{\mathrm{meas.}}$, $\Delta_{\mathrm{natl.}}$, and $\Delta_{\mathrm{m.r.}}$ denoting the FWHM's of the measured, natural, and machine-response line shapes, respectively, we get a convenient ''triangle'' equality of the form

$$\Delta^2_{\mathrm{meas.}} = \Delta^2_{\mathrm{natl.}} + \Delta^2_{\mathrm{m.r.}} \tag{2}$$

to hold. This allows us to remove the effects of the machine response from the fits to our data. A typical fit is shown in Fig. 2. Initial choices for the parameters describing the Gaussians in our analysis were obtained by consideration of the results of Klotz and Peyerimhoff [35]. All parameters were allowed to vary independently.

Once we obtained the fits, we generated cross sections by noting that the latter scale as the scattered-electron current, or area under the excitation line shape. Other factors come in here—such as the scattering geometry, the incident-electron current, and the molecular-beam density of Eq. (1)—but we were able to dispense with them by normalizing to our previous elastic cross section measurements where these effects were already accounted for [20]. The normalization relationship was

$$\left(\frac{d\sigma}{d\Omega}\right)_{\mathrm{inel.}} = \frac{I_{\mathrm{inel.}}\Delta_{\mathrm{inel.}}}{I_{\mathrm{elas.}}\Delta_{\mathrm{elas.}}}\left(\frac{d\sigma}{d\Omega}\right)_{\mathrm{elas.}} \tag{3}$$

where $(d\sigma/d\Omega)_{\mathrm{elas.}}$ and $(d\sigma/d\Omega)_{\mathrm{inel.}}$ are the elastic and inelastic cross sections, respectively, and $I_{\mathrm{elas.}}\Delta_{\mathrm{elas.}}$ and $I_{\mathrm{inel.}}\Delta_{\mathrm{inel.}}$ scale as the areas under their respective line shapes.

Once we obtained absolute differential cross sections, we were able to generate absolute integrated cross sections σ via the relationship

$$\sigma = \int d\varphi\, d\theta \sin\theta \left(\frac{d\sigma}{d\Omega}\right). \tag{4}$$

TABLE V. Absolute cross sections for the excitation of the $c\,^1\Sigma_u^-$ state of molecular oxygen by electron impact. Units for the differential cross sections are $10^{-20}\,\mathrm{cm}^2/\mathrm{sr}$, while those for the integrated cross sections are $10^{-18}\,\mathrm{cm}^2$. Parentheses enclose extrapolated values.

E (eV) \ θ (deg)	12	24	36	48	60	72	84	96	108	120	132	144	156	168	σ
10	(30)	38.6	41.0	40.4	38.2	33.3	40.3	31.9	43.2	41.5	53.1	57.7	51.9	(45)	5.16
15	(15)	15.7	15.8	15.9	23.1	17.8	15.5	11.9	21.5	23.2	27.9	39.6	36.1	(36)	2.44
20	(9.0)	10.4	11.7	9.3	8.3	7.5	8.8	8.3	13.1	13.3	19.0	23.8	26.8	(30)	1.60
30	(3.0)	3.1	2.6	2.5	2.2	2.1	2.4	3.2	3.2	4.7	6.0	7.6	9.9	(10)	0.49

To perform the integrals, we employed the trapezoid algorithm. The integrals required that we extrapolate our differential cross sections to both 0° and 180°, which we did semiexponentially. This introduced uncertainty into our results, but it was minuscule, as the value of $\sin\theta$ in Eq. (4) is very small in the vicinity of these angles.

There were several sources of uncertainty that affected our analysis of the differential cross sections (DCSs), as listed in Table I. Since they were independent of each other, they could be added in quadrature to provide net uncertainties. As the extrapolation to large and small angle introduced negligible uncertainty into the integral cross sections (ICSs), net DCS and ICS uncertainty was about the same.

IV. DISCUSSION OF RESULTS

The pseudocontinuum region of the oxygen molecule's spectrum is especially attractive for electron-collision studies since this molecule's ground X state has unusual $^3\Sigma_g^-$ symmetry, and also because all three transitions to it are electric-dipole forbidden. Excitation of $A\,^3\Sigma_u^+$ is not allowed by the $\Sigma^- \not\to \Sigma^+$ rule, excitation of $A'\,^3\Delta_u$ by the $\Delta\Lambda = 0, \pm 1$ only rule, and excitation of $c\,^1\Sigma_u^-$ by the rule forbidding electron-spin changes. All three also result from the promotion of a $\pi_u 2p$ electron in the ground-state $(\sigma_g 1s)^2(\sigma_u 1s)^2(\sigma_g 2s)^2(\sigma_u 2s)^2(\sigma_g 2p)^2(\pi_u 2p)^4(\pi_g 2p)^2$ configuration to an orbital of $\pi_g 2p$ symmetry.

Our values for the mean excitation energies and slopes for linear approximations to the potential-energy curves in the Franck-Condon region are presented in Table II, where they are compared with the results of Klotz and Peyerimhoff. The form of the potential-energy curves is

$$V = \gamma(r - r_0) + V_0, \tag{5}$$

where r_0 is the equilibrium internuclear distance for O_2 (i.e., the bond length) and has a value of about 1.207 Å. Agreement of the mean excitation energies is encouraging. But the slopes we arrive at give somewhat shallower curves than theirs.

Table III lists the excitation cross sections for the $A\,^3\Sigma_u^+$ state. Figure 3 shows the angular distributions at impact energies of 10, 15, 20, and 30 eV that have a tendency of convergence to zero at extreme angles as predicted by the Σ^--Σ^+ rule for electron-impact excitation [39,40]. (In this and other figures, we show error bars for only selected data points, because providing all error bars would give overly cluttered figures.) The cross sections decrease as the incident energy increases. A minimum appears near 90° at 20-eV impact and near 75° at 30-eV impact.

The cross sections for the excitation of the $A'\,^3\Delta_u$ state are provided in Table IV. Figure 4 shows the differential excitation cross sections at impact energies of 10, 15, 20, and 30 eV. The angular distributions exhibit strong backward scattering. Overall, the cross sections increase toward 15 eV and then decrease at higher energies. There is a broad maximum near 15 eV.

Table V provides the $c\,^1\Sigma_u^-$-state excitation cross sections by electron impact. Figure 5 shows the angular distributions at impact energies of 10, 15, 20, and 30 eV. These are typical for forbidden-state excitation—isotropic angular character with slightly enhanced backward scattering. As the incident energy increases, the overall cross sections become smaller. The forward scattering reduces more than the backward does.

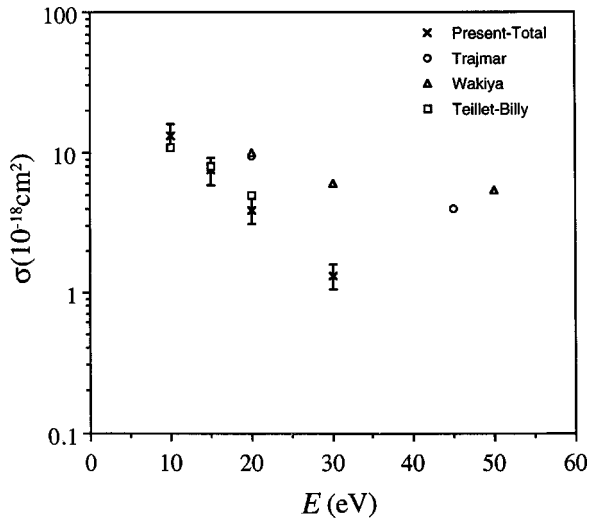

FIG. 7. Absolute integrated cross sections for excitation of the sum of the $A\,^3\Sigma_u^+$, $A'\,^3\Delta_u$, and $c\,^1\Sigma_u^-$ states of molecular oxygen by electron impact. The results of others are also shown. ''Present-Total'' indicates our results, ''Trajmar'' the cross sections of Trajmar, Williams, and Kuppermann, ''Wakiya'' those of Wakiya, and ''Teillet-Billy'' the values of Teillett-Billy, Malegat, and Gauyacq.

Figure 6 shows the excitation ICS's for the three states. For the $A\,^3\Sigma_u^+$ and $c\,^1\Sigma_u^-$ states they decrease exponentially as the incident energy increases. The cross sections of $A\,^3\Delta_u$ state have a broad maximum near 15 eV. The $c\,^1\Sigma_u^-$ state is the largest and the $A\,^3\Sigma_u^+$ state the smallest contributor to the pseudocontinuum's excitation.

Finally, Fig. 7 shows the summed integrated cross sections of three states along with those of Trajmar, Williams, and Kuppermann, of Wakiya, and of Teillet-Billy, Malegat, and Gauyacq. The values of Trajmar, Williams, and Kuppermann, and those of Wakiya are larger than the present results by more than a factor of 2. Those of Teillet-Billy, Malegat, and Gauyacq are in good agreement with the present results. We note, though, that their integral cross sections were obtained as 4π times the measured differential cross sections at 90°.

V. CONCLUSION

We have measured spectra for excitation of O_2's Herzberg pseudocontinuum by electron impact. The spectra were decomposed numerically into contributions from the $A\,^3\Sigma_u^+$, $A'\,^3\Delta_u$, and $c\,^1\Sigma_u^-$ states, resulting in absolute differential cross sections for these states' excitations, along with potential-energy curves in the Franck-Condon region. Integrated cross sections were also obtained.

ACKNOWLEDGMENTS

Support for this research, provided by National Science Foundation Grant No. ATM-9528030, is gratefully acknowledged by the authors. Additional support, provided for one of us by the Brain Pool Project of the Republic of Korea's Government under the supervision of Professor J. S. Chang and Professor J. H. Lee of Seoul National University, is also greatly appreciated.

[1] R. D. Hudson, Rev. Geophys. Space Phys. **9**, 305 (1972).
[2] P. H. Krupenie, J. Phys. Chem. Ref. Data **1**, 423 (1972).
[3] S. Trajmar, D. F. Register, and A. Chutjian, Phys. Rep. **97**, 219 (1983).
[4] S. Trajmar and D. C. Cartwright, in *Electron Molecule Interactions and their Applications*, edited by L. G. Christophorou (Academic, New York, 1984).
[5] Y. Itikawa, A. Ichimura, K. Onda, K. Sakimoto, K. Takanagi, Y. Hatano, M. Hayashi, H. Nishimura, and S. Tsurubuchi, J. Phys. Chem. Ref. Data **18**, 23 (1989).
[6] A. Zecca, G. P. Karwasz, and R. S. Brusa, Riv. Nuovo Cimento **19**, 1 (1996).
[7] G. Herzberg, Naturwissenschaften **20**, 577 (1932).
[8] G. Herzberg, Can. J. Phys. **30**, 185 (1952).
[9] G. Herzberg, Can. J. Phys. **31**, 657 (1953).
[10] A. Konishi, K. Wakiya, M. Yamamoto, and H. Suzuki, J. Phys. Soc. Jpn. **29**, 526 (1970).
[11] K. Wakiya, J. Phys. B **11**, 3913 (1978).
[12] K. Wakiya, J. Phys. B **11**, 3931 (1978).
[13] S. Trajmar, W. Williams, and A. Kuppermann, J. Chem. Phys. **56**, 3759 (1972).
[14] D. Teillet-Billy, L. Malegat, and J. P. Gauyacq, J. Phys. B **20**, 3201 (1987).
[15] C. A. Barth, J. Geophys. Res. **67**, 1628 (1962).
[16] B. H. Solheim and E. J. Llewellyn, Planet. Space Sci. **27**, 473 (1979).
[17] A. W. Yau and G. G. Shepherd, Planet. Space Sci. **27**, 481 (1979).
[18] I. C. McDade, E. J. Llewellyn, R. G. H. Grees, and G. Witt, Can. J. Phys. **62**, 780 (1984).
[19] D. R. Bates, Planet. Space Sci. **36**, 883 (1988).
[20] T. W. Shyn and W. E. Sharp, Phys. Rev. A **26**, 1369 (1982).
[21] T. W. Shyn and W. E. Sharp, Phys. Rev. A **43**, 2300 (1991).
[22] T. W. Shyn and C. J. Sweeney, Phys. Rev. A **47**, 1006 (1993).
[23] T. W. Shyn and C. J. Sweeney, Phys. Rev. A **48**, 1214 (1993).
[24] T. W. Shyn, C. J. Sweeney, and A. Grafe, Phys. Rev. A **49**, 3680 (1994).
[25] T. W. Shyn, C. J. Sweeney, A. Grafe, and W. E. Sharp, Phys. Rev. A **50**, 4794 (1994).
[26] T. W. Shyn, R. S. Stolarski, and G. R. Carginan, Phys. Rev. A **6**, 1002 (1972).
[27] C. J. Sweeney and T. W. Shyn, Phys. Rev. A **53**, 1576 (1996).
[28] C. J. Sweeney and T. W. Shyn, Phys. Rev. A **56**, 1384 (1997).
[29] J. Franck, Trans. Faraday Soc. **21**, 536 (1925).
[30] E. U. Condon, Phys. Rev. **28**, 1182 (1926).
[31] E. U. Condon, Phys. Rev. **32**, 858 (1928).
[32] R. P. Saxon and B. Liu, J. Chem. Phys. **67**, 5432 (1978).
[33] R. P. Saxon and B. Liu, J. Chem. Phys. **73**, 870 (1980).
[34] R. P. Saxon and B. Liu, J. Chem. Phys. **73**, 876 (1980).
[35] R. Klotz and S. D. Peyerimhoff, Mol. Phys. **57**, 573 (1986).
[36] W. H. Press and S. A. Teukolsky, Comput. Phys. **5**, 426 (1991).
[37] W. H. Press, S. A. Teukolsky, W. T. Vetterling, and B. P. Flannery, *Numerical Recipes*, 2nd ed. (Cambridge University Press, Cambridge, 1992).
[38] G. B. Arfken and H. J. Weber, *Mathematical Methods for Physicists*, 4th ed. (Academic, San Diego, 1995).
[39] D. C. Cartwright, S. Trajmar, W. Williams, and D. L. Huestis, Phys. Rev. Lett. **27**, 704 (1971).
[40] W. A. Goddard III, D. L. Huestis, D. C. Cartwright, and S. Trajmar, Chem. Phys. Lett. **11**, 329 (1971).